Variable Processing Shifts during Perceptual Acceleration: Evidence from Temporal Integration

Michael J. Wolff[1] and Elkan G. Akyürek[2]

Abstract

■ The perception of a stimulus can be accelerated by another that precedes it. Perceptual acceleration has been observed in a range of tasks, at varying timescales, and arises by virtue of providing advance spatial and/or temporal information about upcoming stimuli. Here, we examined perceptual acceleration during visual temporal integration. Temporal integration occurs when successive stimuli appear that fit together in time as well as space. As such, stimuli arriving first during temporal integration partially predict those that follow. Although temporal integration is a rapid process, we reasoned that this information may cause perceptual acceleration during temporal integration. We used multivariate pattern analysis of EEG data from a missing element task, designed to measure the visual temporal integration of two successive stimulus displays, so that we were able to precisely track the representation associated with the integrated percept in time. We manipulated the delay between our displays and observed commensurate acceleration of the resultant integrated representation. The degree of acceleration first increased from early (100 msec after stimulus onset) to intermediate (200 msec) processing stages, before decreasing again at a later stage (400 msec). The results thus suggest that perceptual acceleration occurs during temporal integration but is nonlinear, such that some time that is gained at one moment in the process can be lost again at another. ■

INTRODUCTION

We live in the past. As we experience the world around us, our impressions inevitably lag behind the physical reality, because it takes some time to route a signal from our eyes and through the brain. For instance, it takes approximately 120–150 msec to determine basic properties of an unfamiliar natural scene, such as to determine whether it contains an animal or not (Cichy, Pantazis, & Oliva, 2014; Kirchner & Thorpe, 2006; VanRullen & Thorpe, 2001; Thorpe, Fize, & Marlot, 1996). Before that delay has elapsed, higher-level awareness of the contents of the scene is considered to be virtually absent, precluding an appropriate behavioral reaction until perceptual processing is complete. This processing time is nevertheless variable and can be reduced by decreasing the complexity of the scene and the associated task. Furthermore, processing may also be accelerated, if circumstances allow for increased readiness.

Evidence from a range of experimental paradigms has shown perceptual acceleration, typically as a result of providing observers with information about the where and when of upcoming stimuli to prepare for their arrival. Examples of the former include the Posner cueing task (Posner, 1980), in which the RT to a target whose location was validly cued beforehand is reduced, and the so-called rapid resumption in visual search, where search is faster in displays that were previewed before (Spaak, Fonken, Jensen, & de Lange, 2016; Lleras, Rensink, & Enns, 2005). Examples of the latter are studies using temporal cues (Coull & Nobre, 1998), rhythmic presentation sequences (Mathewson, Fabiani, Gratton, Beck, & Lleras, 2010; Jones, Moynihan, MacKenzie, & Puente, 2002), and predictable foreperiods (Luce, 1991), all of which similarly reduce target RT. Here, we hypothesized that such perceptual acceleration may also occur during temporal integration.

Temporal integration is thought to take place during perception, in particular when rapid, successive stimuli fit together, such that they can be combined into a single coherent percept (for a review, see Akyürek, 2025). This is exemplified in the missing element task (MET), which is used to measure visual temporal integration (Akyürek, Schubö, & Hommel, 2010; Di Lollo, 1977, 1980) and which we also used here. The MET commonly entails the presentation of two successive displays, each containing a number of stimuli, which are typically simple shapes such as small squares, circles, or dots, laid out in a regularly spaced grid. Each display only shows half of the stimuli, so that together, the two displays fill up the full grid, apart from a single location in the grid that remains empty (see Figure 1). If this location is found by the observer, this is evidence that the successive stimulus displays were temporally integrated, as working out this location from a mental comparison of the individual displays is very unlikely to succeed.

Although the stimulus displays in the MET are only very briefly shown, within less than 200 msec in total, the first

[1]Ernst Strüngmann Institute for Neuroscience in Cooperation with Max Planck Society, Frankfurt, Germany, [2]University of Groningen

Journal of Cognitive Neuroscience 38:5, pp. 866–879
https://doi.org/10.1162/JOCN.a.2421

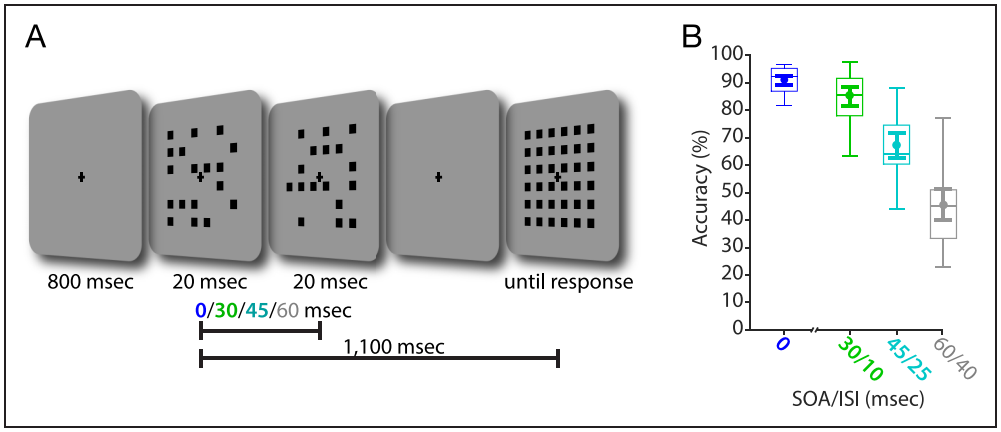

Figure 1. Task structure and behavioral performance. (A) Trial schematic of the MET. After the presentation of an initial fixation cross, 35 of 36 squares on a 6 × 6 grid were presented either at the same time (SOA 0 msec) or across two successive displays (SOA 30, 45, and 60 msec). The response screen was presented after a short delay, and participants clicked on the square they thought was previously missing. (B) Box plots show task accuracy as a function of SOA condition. Center lines indicate the median; box outlines show 25th and 75th percentiles, and whiskers indicate 1.5× the interquartile range. The superimposed filled circles and error bars indicate means and the 95% CI of the means, respectively.

display does provide both spatial and temporal information as to the appearance of the second display. The locations left empty in the first display will be largely filled by the second display (minus the missing element location), and the first display also signals that the second display is going to appear right after. While stimulus timing is very different in the spatial and temporal cueing tasks mentioned above, in those tasks such advance information is known to accelerate perceptual processing. It is thus conceivable that this might also occur in the MET, more so as rapid interactions between its stimuli have some neural plausibility. For instance, one might speculate that the rapid succession of the mutually compatible stimulus displays may cause coincidental neuronal activity, leading to synaptic facilitation through residual elevation of presynaptic Ca^{2+} (Zucker & Regehr, 2002; Markram, Lübke, Frotscher, & Sakmann, 1997). Alternatively, and again speculatively, processing of the first stimulus display in higher-order cells may facilitate processing of the second display in lower-order cells, through back-projections, some of which could operate at MET timescales already (Palmer, Marre, Berry, & Bialek, 2015; Summerfield & Egner, 2009; Friston, 2005).

Using EEG, we could not directly arbitrate between these (or other) neural mechanisms. However, we were able to chart the time course of perceptual acceleration by using multivariate pattern analysis (MVPA) to track the representation of the integrated percept in the brain (van Ede, Chekroud, Stokes, & Nobre, 2018; Marti, King, & Dehaene, 2015), as a first step in helping to constrain the range of possible underlying neural mechanisms. Other than expecting evidence for a degree of perceptual acceleration during temporal integration, we did not have strong expectations as to its precise time course. Evidence from cueing, rhythm, and foreperiod studies does not strongly suggest a particular temporal locus. Spatial cueing affects early perceptual processing stages, as it is accompanied by amplitude (but not latency) modulations of the P1 and N1 components of the ERP (Mangun, 1995; Mangun & Hillyard, 1991). Advance temporal information has been found to modulate the N1 (Seibold & Rolke, 2014), N2 (Seibold, Fiedler, & Rolke, 2011), P3 (Griffin, Miniussi, & Nobre, 2002), as well as slow potentials and oscillatory components (Rohenkohl & Nobre, 2011; Praamstra, Kourtis, Kwok, & Oostenveld, 2006). Apart from this already wide temporal range, it is difficult to relate univariate electrophysiological measures to perceptual acceleration directly, as they reflect both perceptual and cognitive processing as well as the representations they act on. Thus, we did not constrain our analyses to a specific time window but relied on MVPA to focus on the representation of the missing element itself, to chart when that representation arises, as a function of our task parameters.

The Current Study

As indicated, we used a MET to assess perceptual acceleration. We manipulated the SOA between the displays in our MET, measured the EEG, applied MVPA to decode the location of the missing element, and compared its occurrence in time between conditions by means of cross-temporal generalization. To preview the results, we found evidence for accelerated perceptual processing during temporal integration, but also observed that this acceleration varied over time as the missing element was being processed in the brain, such that initial gains were partially lost again later in that process.

METHODS

Participants

Twenty-four first-year psychology students of the University of Groningen (nine female, mean age = 21 years, range = 18–28 years) were included in the analyses. Eight additional participants failed to meet the previously set inclusion criterion (80% accuracy on the SOA 0/no integration condition), and their data were discarded during collection. The final sample size of 24 was decided on before data collection and is based on a previous study that used a

similar EEG analysis pipeline to decode visual stimuli (Wolff, Ding, Myers, & Stokes, 2015). Participants received course credits for participation and gave written informed consent. The study was approved by the ethics committee of the Psychology department of the University of Groningen (approval no. 16340-S-NE).

Apparatus and Stimuli

Stimuli were controlled and generated with Psychtoolbox (Kleiner, Brainard, & Pelli, 2007), a freely available toolbox for MATLAB (The MathWorks), and presented on a 19-in. (48.3-cm) CRT screen running at 200-Hz refresh rate and a resolution of 640 by 480 pixels. Responses were made with a conventional computer mouse. Participants were seated approximately 64 cm from the monitor. The stimuli consisted of black squares (0.72°) arranged in a 6 by 6 grid (7.92°) in the center of the screen. The empty spaces between squares were the same size as the squares themselves (0.72°). A black fixation cross (0.97°) and a gray background (red, green, blue = 150, 150, 150) were maintained throughout the trials.

Procedure

Each trial began with the presentation of a fixation cross. After 800 msec, 35 of 36 black squares, arranged on a 6 by 6 grid, were presented either at the same time (SOA = 0 msec) or across two successive displays, for 20 msec each, with an ISI of 10, 25, or 40 msec (SOA = 30, 45, or 60 msec). Participants were instructed to locate the one missing square, which could be anywhere within the inner 4 by 4 grid, and of which they were made aware beforehand. Note that in order to detect the missing square, both displays need to be temporally integrated by the perceptual system, which is more difficult at longer SOAs (Di Lollo, 1977; Hogben & di Lollo, 1974). The response screen was presented 1100 msec after the onset of the first display and consisted of the whole grid of squares. Participants used the mouse cursor to click on the square that they thought was previously missing. Immediately after their response, the correct square flashed in green, and, if incorrect, the chosen square in red. Participants completed 1056 trials in total, over a course of approximately 75 min, including breaks. See Figure 1A for a trial schematic.

No integration (SOA 0) trials made up 27%, SOA 30 trials made up 27%, and SOA 45 and SOA 60 made up 36% and 9% of all trials, respectively. SOA 45 made up the largest proportion of trials due to the anticipated difficulty of this condition. Of the most difficult condition of SOA 60, only a small number of trials were included in the experiment. These served merely to confirm the expected decrease in accuracy as a function of SOA due to temporal integration eventually breaking down, as has previously been observed (e.g., Akyürek et al., 2010), and this SOA was excluded from all neurophysiological analyses.

Electrophysiological Recording and Preprocessing

The EEG signal was acquired from 59 Ag/AgCls sintered electrodes laid out according to the extended international 10–20 system (Supplemental Figure S1A), with two additional electrodes placed on the mastoids. Another electrode, placed above the sternum, was used as ground. Four electrodes placed above and below the left eye and on the temples recorded the bipolar EOG signals. The data were recorded with a TMSI Refa8-64/72 amplifier, sampling at 1024 Hz with an average reference. Impedances were kept below 10 kΩ. Offline, the data were re-referenced to the average of both mastoid electrodes and filtered with a 0.05-Hz high-pass and a 40-Hz low-pass filter. Only the 24 posterior EEG channels (P7, P5, P3, P1, Pz, P2, P4, P6, P8, PO7, PO3, POz, PO4, PO8, O1, Oz, O2, P9, PO9, O9, Iz, O10, PO10, and P10) were included in all following preprocessing steps and analyses (unless otherwise specified), as we expected the relevant visual signal to be the strongest in these channels, which cover parietal and occipital cortex. This decision was made a priori and based on our previous experience involving visual tasks and multivariate pattern analyses, where also only the posterior channels were included (e.g., Wolff, Jochim, Akyürek, Buschman, & Stokes, 2020; Wolff, Jochim, Akyürek, & Stokes, 2017; Wolff et al., 2015), which is a practice also used by others (e.g., Kandemir & Olivers, 2024; Harrison, Bays, & Rideaux, 2023). The data were epoched relative to the onset of the first display (−250 to 1100 msec) and baseline-corrected using the mean signal from −250 to 0 msec relative to Display 1 onset. Noisy trials and trials containing ocular artifacts were identified by visually inspecting the EEG and EOG signal and removed from the analyses.

Location Decoding

We were interested in the time course of the location code of the missing square in the EEG signal. We used Mahalanobis distance (De Maesschalck, Jouan-Rimbaud, & Massart, 2000) to test if the signal contained information about the location at any one point throughout the trial. We used custom MATLAB code as well as functions from the Statistics and Machine Learning Toolbox for MATLAB. The above-listed 24 posterior channels were included in the decoding analyses. In essence, we tested if same-location trials were closer to each other in multidimensional space (i.e., a shorter Mahalanobis distance) than different-location trials, where each EEG channel is a separate dimension. Mahalanobis distance is similar to Euclidean distance, but it considers the covariance between dimensions/EEG channels and can substantially improve decoding performance, in particular when used on EEG data with highly correlated EEG channels. The EEG data were first smoothed with a Gaussian smoothing kernel (SD = 10 msec) along the time dimension and mean-centered across channels prior to analysis. Using an eightfold cross-validation approach, the trialwise

Mahalanobis distances between train trials and the left-out test trials was computed at each time point separately using the MATLAB function *pdist2* from the Statistics and Machine Learning Toolbox. The covariance matrix was computed at each time point using all train trials with a shrinkage estimator using custom MATLAB code (Ledoit & Wolf, 2004). This procedure was repeated 50 times, each time randomly partitioning the data into eight folds. Same-location distances were subsequently subtracted from the average of all different-location distances, such that a positive "distance difference" represents a shorter distance between trials that had the same missing square locations than between trials that had different locations, similar as was done previously for orientation decoding (Wolff et al., 2015), suggesting that the electrophysiological signal contains location-specific information. We ran this analysis separately for the three conditions of interest (SOA 0, SOA 30, and SOA 45), and for completeness, we repeated the same analyses including all 59 EEG channels.

For visualization purposes, we complemented the temporal decoding analysis with a searchlight decoding analysis where the decoding was repeated iteratively for a subset of electrodes across all 59 electrodes. For each iteration, the current as well as the closest two neighboring electrodes were included (similar to van Ede, Chekroud, Stokes, & Nobre, 2019). This was done separately for each previously identified processing stage (90–140, 140–300, 300–500, and 500–1100 msec). Within each time window, information was pooled across time to take advantage of the fact that information is also contained in the temporal profile of the data, for which we used a previously used approach (Wolff et al., 2020). That is, for a given time window, the data of the three channels in question were first downsampled to 102.4 Hz (by taking the average of 10 consecutive time points) and then added as additional dimensions to the decoding analysis. For example, for the early time window (90–140 msec), there were five time points per channel, which resulted in 15 dimensions for the subsequent decoding analysis (3 channels × 5 time points), which was otherwise the same as described as above. The MATLAB extension fieldtrip (Oostenveld, Fries, Maris, & Schoffelen, 2010) was used to visualize the decoding topographies.

Cross-temporal Decoding

We were interested in the neural dynamics of the processing of the missing square. Instead of training and testing the classifier on the same time points as described above, in cross-temporal decoding analyses, the classifier is trained and tested on all possible time point combinations, resulting in a full cross-temporal decoding matrix (King & Dehaene, 2014). The cross-temporal dynamics were tested for significance using the same method as in Myers et al. (2015): The decodability at each cross-temporal time point $t_{x,y}$ to the corresponding time points on the diagonal ($t_{x,x}$ and $t_{y,y}$). A significant difference in both was taken as evidence for dynamic coding. A cluster-based permutation test was used to correct for multiple comparisons.

Finally and most importantly, we wanted to test to what extent the processing of the missing square location is temporally shifted when the necessary visual information is not presented simultaneously, as in the SOA 0 condition but spread across two discrete displays, as in the SOA 30 and SOA 45 conditions. To do so, we used the same decoding approach as described above, but instead of using cross-validation with separate train and test folds of the same SOA condition, we trained the classifier on the SOA 0 condition and tested it separately on both the SOA 30 and SOA 45 conditions. As we did not know to what extent the visual processing of the missing square is temporally shifted between the SOA 0 condition and the two integration conditions (e.g., it could be time-locked to the first or the second display, or somewhere in between), we obtained the full cross-temporal decoding matrix as described above.

Quantifying the Temporal Shift

We wanted to quantify the possible temporal shift obtained from the cross-temporal and cross-condition decoding matrices, where the classifier was trained on the no-integration condition (SOA 0) and tested on each temporal integration (SOA 30 and SOA 45, see above). To quantify this shift, we developed an analysis that assumes that a dynamic, cross-temporal decoding profile is symmetric around the true temporal offset. First, the dynamics of the decoding matrices were normalized at each time point by z scoring the decoding values across both the x and y axes of the matrices and then averaging them. Then, a centered 50-msec sliding window approach was used to determine the temporal shift. At each time point along the diagonal (from 90 msec, the onset of reliable decoding in the SOA 0 condition, to 500 msec), the average of all decoding values in the upper triangle was subtracted from the average of the lower triangle. This sliding window was moved up and down the training and testing axes of the decoding matrix. Zero difference at a specific offset indicates that the cross-temporal decoding window is symmetrical at this offset, whereas a positive or negative difference provides evidence for a temporal shift in the corresponding direction.

The "shift score" was computed using the following formula:

$$s_{t,o} = \frac{\begin{array}{c}(L(t_{\text{trn}}, t_{\text{tst}} + o) - U(t_{\text{trn}}, t_{\text{tst}} + o)) \\ + (L(t_{\text{trn}} - o, t_{\text{tst}}) - U(t_{\text{trn}} - o, t_{\text{tst}}))\end{array}}{2}$$

$$s_{t,o} = \frac{\left(L1_{t,o} - U1_{t,o}\right) + \left(L2_{t,o} - U2_{t,o}\right)}{2}$$

where t_{trn} and t_{tst} are the time points along the training and testing axis, respectively, both relative to the onset of

the first display ($t_{trn} = t_{tst}$); U and L are the means of the upper and lower triangle of the 50-msec sliding window, respectively; o is the temporal offset of the sliding window (in msec) relative to t; and s is the shift score.

Identifying Distinct Stages of Location Processing

The time course of decoding and the cross-temporal decoding matrix of the no-integration condition were compared with the ERP to identify different stages in processing of the location of the missing element. Stages were characterized on the basis of the correspondence observed between ERP component amplitude, decoding accuracy, and (switches between) periods of dynamic and stable coding. The identification of these stages was not necessarily meant to strictly delineate separable or independent processes but to provide a handle on different moments within the perceptual process.

SOA 0 to Display 1 Location Generalization

In light of the results, it could be argued that Display 1 alone in the temporal integration conditions provides partial information of where the missing element is going to be (i.e., all empty locations), before Display 2 is even presented. This could in turn be picked up by the decoder as an earlier than expected signal of the missing element, which could (at least in part) occur before Display 2 is even processed and temporally integrated with Display 1 by the brain. To this end, we attempted to test if, and to what extent, the signal of the missing element location in the SOA 0 condition generalizes with empty locations in Display 1 that are not the missing element in the integration conditions.

This would mean that the signal of the missing element location in the SOA 0 should be similar with the signal of trials from an integration condition (SOA 30 and SOA 45) when the same location is empty at Display 1 but is occupied by Display 2 (meaning that it is not actually the missing element location in those trials), compared with trials where it is the other way around (location occupied at Display 1, but empty at Display 2; see Supplemental Figure S4A for a schematic). Thus, if the empty locations in Display 1 leads to a prediction of where the missing element could be that results in a measurable signal, which generalizes with signal of the SOA 0 condition, then the trials this applies to (Display 1 empty) should be more similar (shorter Mahalanobis distance) to the corresponding SOA 0 trials than the trials this does not apply to (Display 1 occupied and Display 2 empty).

This is exactly what we tested. Specifically, from the SOA 0 condition, we first computed the covariance matrix using all trials before the signal was averaged over trials based on the missing element locations (just like before). Next, the distance difference between Display 1 empty and Display 2 empty of a specific temporal integration condition was computed for all missing element locations. For example, say for the missing element Location 5 in the SOA 0 condition, the signal of trials of a given integration condition were averaged based on whether Location 5 was empty in Display 1 "or" in Display 2 (but never both). The distance to the average signal of each group of trials was then computed between the average signal over all missing element Location 5 trials in the SOA 0 and the two trial types of a given integration condition. Then, the distance difference was computed, where the distance to the Display 1 empty trials was subtracted from the distance to the Display 2 empty trials. The same was repeated for all 16 missing element locations, each time averaging the trials of the integration condition based on whether the corresponding location was empty at Display 1 or 2, before the average distance difference (Display 1 empty − Display 2 empty) was obtained. This was done for each time point, where the signal of the SOA 0 condition was time-locked to the onset of the only display and the signal of the integration conditions was time-locked to the onset of Display 1. This procedure was done separately for the SOA 30 and SOA 45 conditions.

Significance Testing

We used nonparametric permutation tests for all statistical analyses. In subject analyses, for each subject, the sign of the decoding or the deviation of the "shift score" from the temporal offset in question was randomly flipped at each time point 10,000 times. The resulting null distribution was used to derive the p value. Cluster-based permutation tests were used to correct for multiple comparisons across the time dimension(s) using 10,000 permutations, with a cluster-forming threshold of $p < .05$. Statistical significance was set at $p < .05$. All tests were two-sided. Additionally, Bayes factors (BF) were obtained for the average "shift score" deviations at each processing stage, as well as for each time point and temporal offset (the latter only for visualization). For this, we performed Bayesian t tests with the default Cauchy prior scale of 0.707 (Rouder, Speckman, Sun, Morey, & Iverson, 2009).

Decoding topographies were tested for significance using the cluster-based permutation for channels as implemented by the MATLAB extension fieldtrip (Oostenveld et al., 2010), where instead of testing for significant decoding clusters over time (as described above), the topographies were tested for significant decoding clusters across space. The neighbors for each channel were first defined using the triangulation method of the fieldtrip function "ft_prepare_neighbours." Then electrode clusters with significant decoding were obtained for each time window of interest using the Monte Carlo method with 10,000 permutations, a cluster-forming threshold of $p < .05$, and a minimum of two neighboring channels for a sample to be included in the clustering.

Group-level analyses were used to estimate the temporal shift at each specific processing stage (detailed below) and SOA condition. The mean temporal shift values were sampled with replacement from each time window of

interest, and the shift was computed 5000 times. The resulting distribution was used to compute the 95% CI.

Differences between SOAs and processing stages were also tested on the group level by randomly flipping the condition labels of each subject with .5 probability, before computing the mean difference 10,000 times. The null distribution was used to calculate the proportion of permutations more extreme than the actual group-level difference. Statistical significance was set at $p < .05$. Tests between SOA conditions were one-sided, testing specifically if the temporal shift in the SOA 45 condition was larger than in the SOA 30 condition. These tests were one-sided, as greater SOA would never be expected to reduce temporal shift, and vice versa. The p values of all possible pairwise differences between processing stages were Bonferroni-corrected for multiple comparisons and were two-sided.

RESULTS

Behavioral

Figure 1B shows a clear negative effect of increasing SOA on the behavioral accuracy of locating the missing square ($p < .001$ of all pairwise comparisons, two-sided, Bonferroni-corrected). This suggests that the two displays are less likely to be temporally integrated at longer SOAs, leading to worse performance, which replicates previous findings (Akyürek et al., 2010; Di Lollo, 1977).

Distinct Stages of Location Processing

We used the SOA 0 condition as a "template" to define the time windows of individual processing stages and to test the neural dynamics of location processing. The decoding time course showed a significant cluster from 91 to 1100 msec (end of epoch), relative to display onset ($p < .001$, cluster-corrected), providing evidence that the location of the missing square was decodable from the EEG shortly after stimulus presentation (Figure 2A). The SOA 30 and SOA 45 conditions showed similar but weaker decoding profiles (Supplemental Figure S1), likely due to the weaker percept of the missing element and lower behavioral accuracy in these conditions.

The cross-temporal decoding matrix of the SOA 0 condition showed that approximately 140 msec after stimulus onset training and testing trials cross-generalized significantly, while at the same time providing evidence for a highly dynamic code from decoding onset until approximately 500 msec after onset (decoding cluster: $p < .001$; dynamic coding cluster: $p < .001$, both cluster-corrected; Figure 2B). Visual inspection of the one-dimensional and two-dimensional decoding time courses, in conjunction with the significant clusters of decoding and dynamic coding, suggested four distinct processing stages, which corresponded well with the averaged evoked potentials (Figure 2C).

1. An early location-specific response from approximately 90 to 140 msec, which did not cross-generalize with

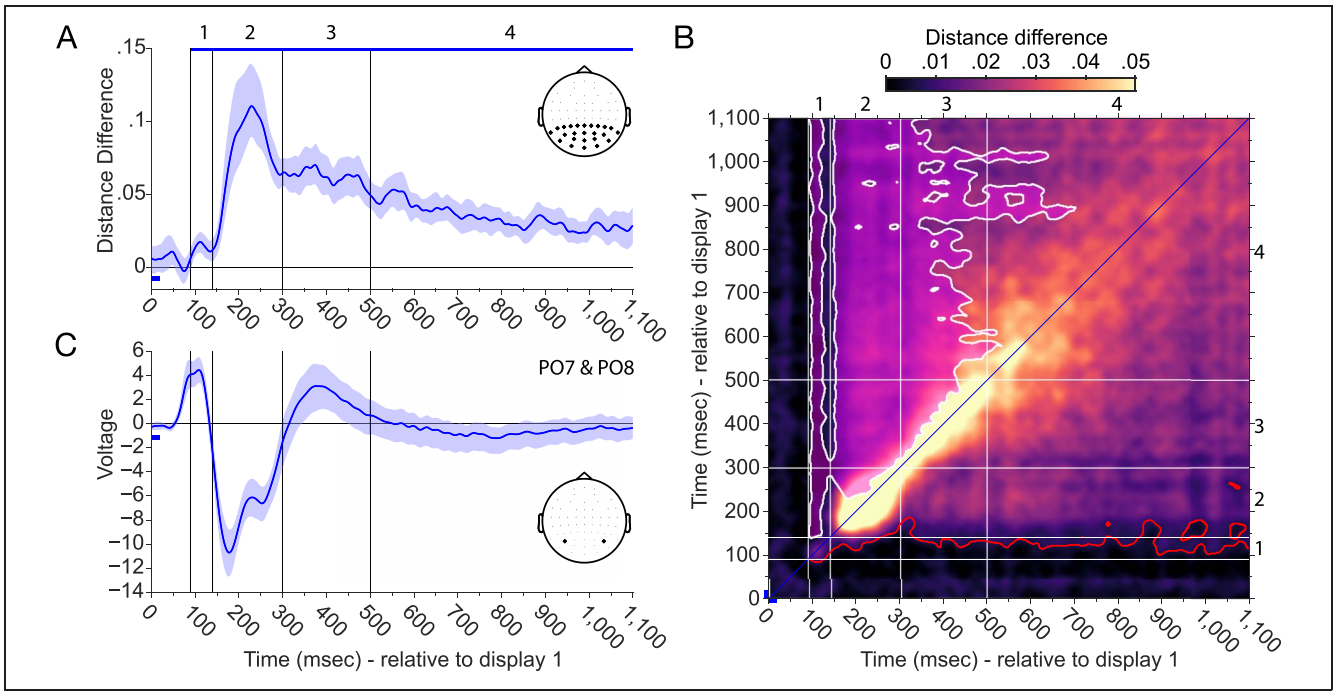

Figure 2. Identifying distinct processing stages. (A) Decoding time course of the location of the missing square in the SOA 0 condition using the posterior electrodes. Blue bar on top indicates significant decoding ($p < .05$, cluster-corrected). Blue bar on the bottom left indicates Display 1 presentation. Error shading indicates the 95% CI of decoding accuracy. Black vertical lines and numbers indicate distinct processing stages (see text). (B) Cross-temporal decoding matrix of the SOA 0 condition. The white outline depicts time points of significantly lower decoding than for both equivalent time points along the diagonal, providing evidence for dynamic coding ($p < .05$, cluster-corrected). The red outline indicates time points of significant decoding ($p < .05$, cluster-corrected). (C) Average evoked potential from the electrodes PO7 and PO8 with 95% CI (blue shading).

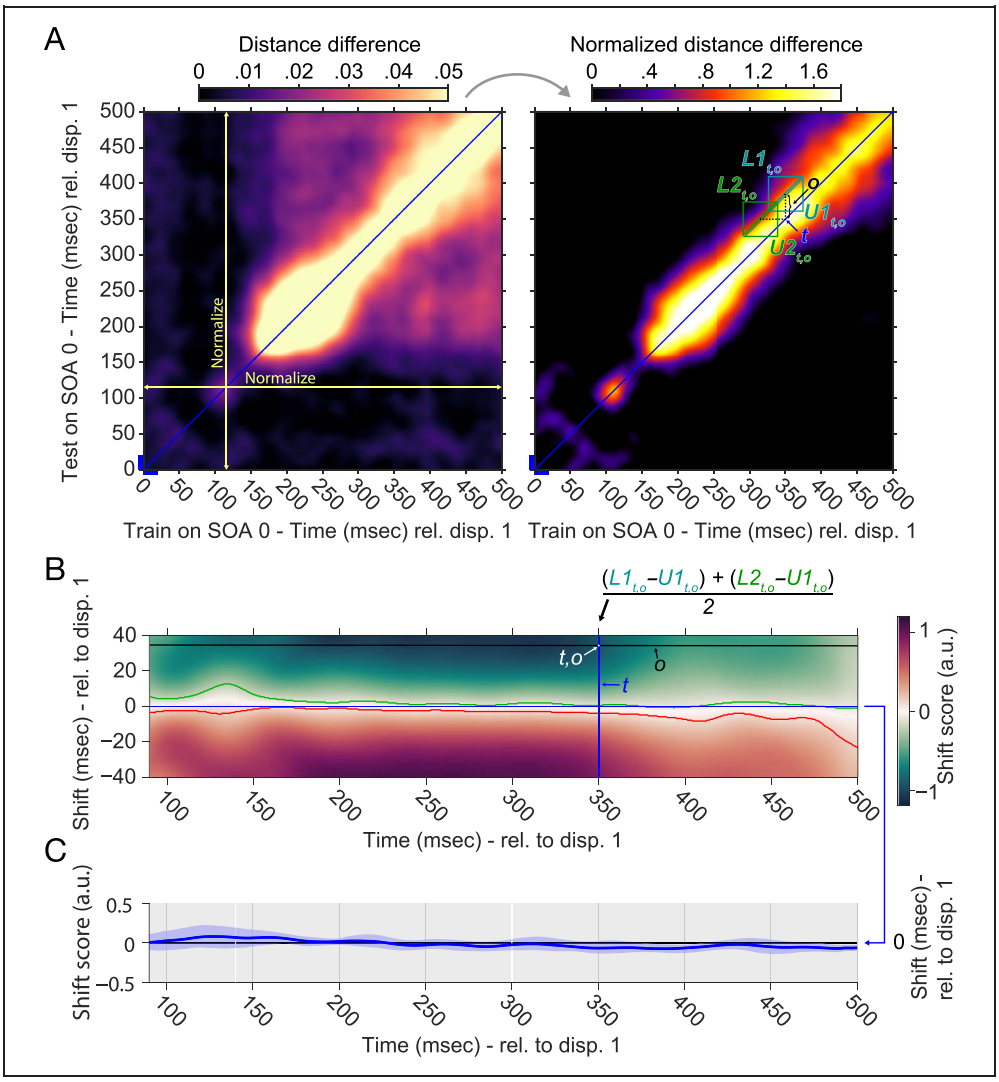

Figure 3. Demonstration of "shift score" computation. (A) Cross-temporal decoding matrix of the SOA 0 condition (left). Yellow lines visualize normalization across cross-temporal time dimension. Normalized decoding matrix by z scoring decoding values along the cross-temporal time-dimensions (right). Computation of shift score at a specific time (t) and temporal offset (o) is illustrated. (B) Shift scores with temporal offsets from −40 to 40 msec. Negative values suggest higher decodability at shorter offsets; positive values suggest higher decodability at longer offsets. Green and red outlines depict significantly negative and positive shift score clusters ($p < .05$), respectively. (C) Shift score at 0-msec temporal offset with 95% CI. No evidence of significant deviation was found ($p > .2$, cluster-corrected), suggesting that the neural dynamics are centered at 0 (as expected).

any subsequent time points. The decoding time course overlapped with the P1, which is known to be modulated by early attentional filtering and stimulus selection (Hillyard, Teder-Sälejärvi, & Münte, 1998) and which originates in V2 (Woldorff et al., 1997).

2. High decodability from 140 to 300 msec, overlapping with the time course of the N1 and N2, likely reflecting the attentional shift toward the location of the missing square (Patel & Azzam, 2005) and spatial grouping (Akyürek et al., 2010).
3. Highly dynamic location decoding from 300 to 500 msec, overlapping with the time course of the P3, likely reflecting the consolidation of the missing square location in working memory, and processes related to response selection (Polich, 2007; Verleger, Jaśkowski, & Wascher, 2005).
4. Stable and relatively low decoding from 500 to 1100 msec (end of epoch), likely reflecting the continuous maintenance of the missing square location in working memory, possibly related to the contralateral delay activity component (Akyürek, Kappelmann, Volkert, & van Rijn, 2017; Vogel & Machizawa, 2004).

Since we were interested in the temporal shift of the dynamic brain states between no integration and integration, we focused on the dynamic time window up to 500 msec after stimulus presentation for all subsequent analyses, excluding the stable maintenance period.

Searchlight decoding analyses over electrode clusters of the SOA 0 condition for each processing stage showed that decoding was generally most robust in posterior electrodes (Supplemental Figure S2); this, in conjunction with lower decoding when using all electrodes for decoding (Supplemental Figure S1B), corroborates our a priori choice to only use the posterior electrodes for the main analyses.

Exemplifying "Shift Score" Computation on SOA 0

We quantified the mid-point of the cross-temporal decoding matrix relative to the diagonal by computing the shift score. Here, we demonstrate this analysis on the cross-temporal decoding matrix of the SOA 0 condition, where we do not expect a systematic deviation from diagonal, since both training and testing come from the same SOA 0 condition. The method is described above ("Quantifying

the temporal shift") and illustrated in Figure 3. A significance test on the shift score matrix reveals one negative and one positive cluster of shift score values ($p < .001$, cluster-corrected; Figure 3B). Neither of the clusters cross the 0 line, demonstrating that while there is no evidence for a temporal shift when training and testing at the same time points, the shift score analysis is sensitive enough to pick up the asymmetry of the decoding matrix when separating training and testing by as little as ~5 msec. The 0-msec offset was explicitly tested for significant deviations of the shift scores. As expected, no significant clusters were detected ($p > .2$, cluster-corrected; Figure 3C).

Temporally Shifted Neural Dynamics of Location Processing during Temporal Integration

The neural dynamics of missing square location processing in the SOA 0 condition cross-generalized significantly with both temporal integration conditions ($p < .001$ of both cross-temporal decoding clusters; Figure 4A and B), with similar neural dynamics across the whole time window as SOA 0 (see Figure 3A). However, a temporal shift seemed to be present in both temporal integration conditions, as the decoding dynamics were not symmetrical along the diagonal (training at testing at the same time points, relative to Display 1 onset).

Two clusters of significant shift scores were present in the SOA 30 condition, one negative and one positive (both $p < .001$, cluster-corrected; Figure 4C). For the most part, the point of decoding symmetry (shift score = 0) was wedged between the onset of Display 1 (0 msec) and Display 2 (30 msec), constituting evidence for perceptual acceleration during temporal integration. A positive and negative shift score cluster were also present in the shift score matrix of the SOA 45 condition (both $p < .001$, cluster-corrected; Figure 4D). Like SOA 30, the point of

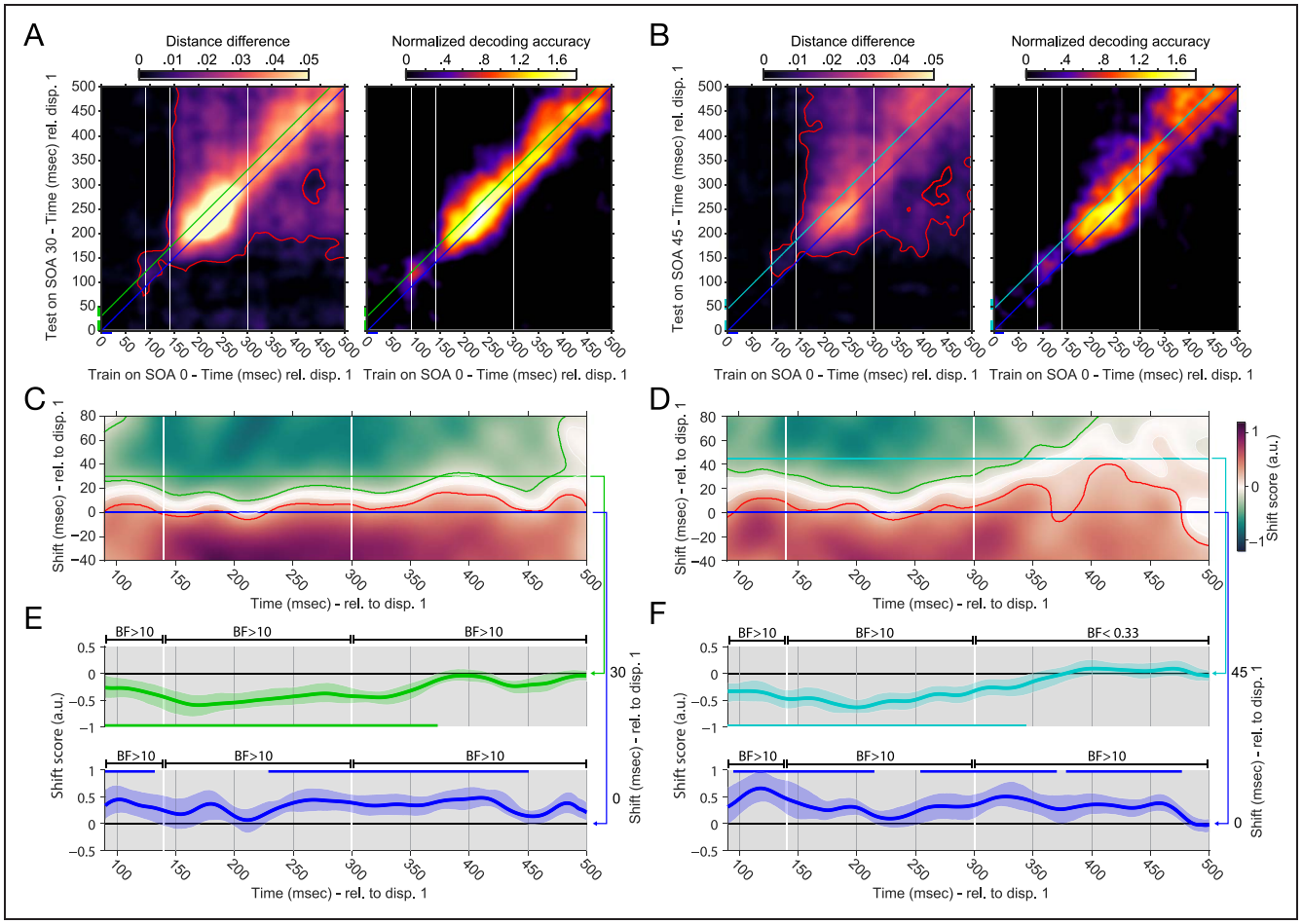

Figure 4. Accelerated location processing during temporal integration. (A) Cross-temporal generalization matrix between SOA 0 and SOA 30. White lines indicate previously defined processing stages. Left: The red outline indicates time points of significant cross-generalization ($p < .05$, cluster-corrected). Right: Normalized generalization matrix. (B) Cross-temporal generalization matrix between SOA 0 and SOA 45. (C and D) Shift scores of normalized cross-temporal generalizations between SOA 0 and SOA 30, and SOA 0 and SOA 45, respectively. Green and red outlines depict significantly negative and positive shift score clusters ($p < .05$), respectively. White outlines and shading show shift scores with strong evidence against a positive or negative deviation (i.e., evidence for no deviation), representing the estimated temporal shift of processing (Bayes factor < 0.333). (E) Shift scores of SOA 30 at 30 msec (green) and 0 msec (blue) temporal offset. Bars in the corresponding colors show significant shift scores ($p < .05$, cluster-corrected). Error shading indicate 95% CI of the mean. Approximate Bayes factors (*BF*) are shown for the average shift scores of each processing stage. (F) Shift scores of SOA 45 at 45 msec (cyan) and 0 msec (blue) temporal offset. Same convention as (E).

symmetry was largely between the onsets of the first and second displays, though the acceleration during integration seemed to diminish toward the end of the dynamic time window.

We explicitly tested if there was evidence for a temporal shift at the temporal onsets of the first (0 msec) and the second display (30/45 msec) in both temporal integration conditions. In the SOA 30 condition, this revealed a significant negative shift score cluster at a temporal offset of Display 2 onset/30 msec ($p < .001$, cluster-corrected; Figure 4E, top), providing evidence for a temporal offset of the neural dynamics that is less than the SOA between displays (30 msec). Two positive shift score clusters were present at 0-msec temporal offset ($p = .043$ and $p < .001$, cluster-corrected; Figure 4E, bottom), indicating that location processing is delayed during temporal integration relative to Display 1 onset. The SOA 45 condition showed a similar pattern of results. One negative shift score cluster was present at a temporal offset of Display 2/45 msec ($p < .001$, cluster-corrected; Figure 4F, top), as well as three positive clusters at 0-msec temporal offset ($p < .001$, $p < .001$, and $p = .004$, cluster-corrected; Figure 4F, bottom).

Bayesian analyses performed on the average shift scores over the temporal windows of each previously defined processing stage showed strong evidence for positive shift scores in the SOA 30 condition relative to a 0-msec temporal offset (90–140 msec, $BF = 19.139$; 140–300 msec, $BF = 55.147$; 300–500 msec, $BF > 10{,}000$) and strong evidence for negative shift scores relative to a 30-msec temporal offset (90–140 msec, $BF = 27.586$; 140–300 msec, $BF > 1000$; 300–500 msec, $BF > 1000$). The results for the SOA 45 condition showed strong evidence for positive shift scores relative to a 0-msec offset (90–140 msec, $BF = 63.831$; 140–300 msec, $BF > 1000$; 300–500 msec, $BF > 1000$). While there was also strong evidence for negative shift scores relative to a 45-msec offset for the first two stages (90–140 msec, $BF = 170.117$; 140–300 msec, $BF > 1000$), there was evidence "against" a shift score deviation for the last stage of interest (300–500 msec, $BF = 0.278$).

In summary, when Display 2 was delayed, processing of the missing element location was also delayed, compared with the SOA 0 condition (Figure 4E and F, bottom). However, it was not delayed as much as would be expected from the SOA (i.e., 30 or 45 msec) between displays (Figure 4E and F, top). That means that the processing of the missing element was actually accelerated in these integration conditions, in particular during the early processing stages.

Distinct Temporal Shifts of Location Processing Stages during Temporal Integration

Average temporal shifts at each previously defined processing stage are shown in Table 1 and Figure 5. Apart from one exception, all CIs of the temporal shifts fell in between the onsets of Displays 1 and 2. Group analyses showed that while the temporal shift was not significantly higher in the SOA 45 condition than the SOA 30 condition in the early processing stage (90–140 msec, $p = .099$), its average shift was higher in both the middle (140–300 msec, $p = .021$) and late processing stages (300–500 msec, $p < .001$).

Pairwise comparisons between processing stages (averaged across both conditions) revealed that the temporal shift at the middle processing stage was significantly lower than at both the early and late processing stages ($p = .004$ and $p = .001$, respectively, Bonferroni-corrected), while the temporal shifts at the early and late stages did not differ significantly ($p > .5$, Bonferroni-corrected).

Results obtained when using all EEG channels for the previous decoding procedures were qualitatively similar, though the difference between temporal shifts of the SOA conditions at the middle processing stage was not significant (Supplemental Figure S3).

No Evidence that Partial Display 1 Information Generalizes with SOA 0 Decoding

It could be argued that the previously reported results may not necessarily be due to accelerated perception during visual temporal integration, but rather because the presentation of the first display alone already provides partial information about where the missing element is going to be. If so, the signal associated with empty locations at

Table 1. Temporal Shifts of Location Processing Dynamics as a Function of Temporal Integration Condition (SOA 30/SOA 45) for Each Processing Stage

Time Condition	*90–140 msec*	*140–300 msec*	*300–500 msec*
SOA 30	17 msec	10 msec	18 msec
	[10, 23]	[6, 13]	[14, 21]
SOA 45	24 msec	15 msec	40 msec
	[13, 33]	[10, 20]	[28, 55]

95% CIs are shown in brackets.

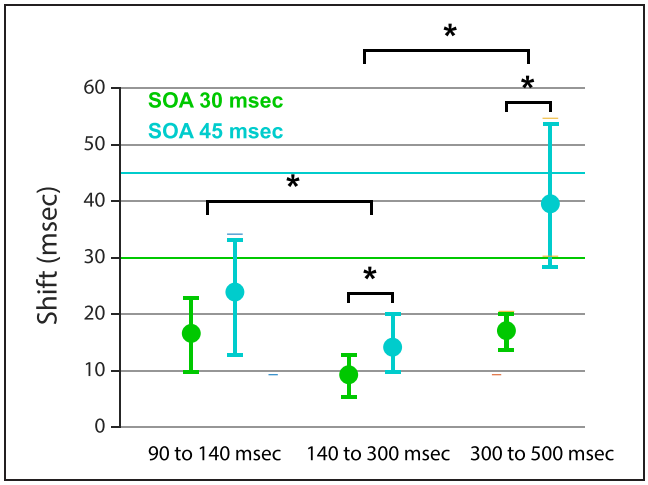

Figure 5. Temporal shifts of location processing dynamics. Error bars are 95% CIs. Asterisks denote significant differences between SOAs and processing stages ($p < .05$, Bonferroni-corrected for comparisons between stages).

Display 1 in the integration conditions (SOA 30 and SOA 45) should generalize with the signal of the missing element location in the SOA 0 condition (for a more detailed explanation, see Methods and Supplemental Figure S4A). However, we found no evidence that this was the case for either the SOA 30 or the SOA 45 condition (Supplemental Figure S4B).

DISCUSSION

We decoded the location of the missing element from EEG recorded in the temporal integration task that bears its name. This location is only apparent when the two successive stimulus displays in the MET are temporally integrated into a single perceptual representation, thus providing a highly time-sensitive fingerprint that can be tracked in the brain. We observed that perception is accelerated during temporal integration: The location of the missing element could be decoded sooner than would be expected on the basis of the actual delay between the stimulus displays. Compared with simultaneous presentation of the displays, the missing element was delayed by only 15 msec on average at an SOA of 30 msec (corresponding to an acceleration of 15 msec also). At an SOA of 45 msec, the missing element was delayed by only 26 msec on average (19-msec acceleration). These results constitute evidence that the perception of the first display facilitated that of the second, thereby possibly aiding in their joint integration. This evidence of perceptual acceleration during temporal integration places our fast-paced task within a larger family of spatial/temporal cueing (Coull & Nobre, 1998; Posner, 1980), rapid resumption (Spaak et al., 2016; Lleras et al., 2005), foreperiod (Luce, 1991), and rhythmic tasks (Mathewson et al., 2010; Jones et al., 2002), in which advance information aids the observers in perceiving and acting more quickly.

Importantly, we also observed that acceleration varied depending on the precise moment in the perceptual processing pathway. Combined across SOAs, processing was accelerated by 17 msec in the early stage, by 25 msec in the middle stage, and by 9 msec in the late stage. Thus, perceptual acceleration was neither linear, nor constant, but variable to the extent that early gains were at least partially lost again later. The observed nonuniformity might be conceptualized as a queuing effect that may happen when information is passed from one stage to another, such that rapid completion of processing in one stage may be followed by increased waiting time for the next stage. In other words, as information flows from one processing stage to the next, it can wax as well as wane.

The Locus of Perceptual Acceleration

In our experimental task, processing the second display was facilitated only by the onset of the first, less than 50 msec prior, which is an interval that has been considered too short to afford proper temporal preparation (Los & Schut, 2008). Indeed, at this temporal offset, the acceleration effect would seem to be driven purely by low-level factors within local neuronal assemblies in early visual cortex, such as synaptic facilitation (Zucker & Regehr, 2002; Markram et al., 1997). From this perspective, it is all the more surprising that the acceleration effect on the resultant representation was not straightforward (i.e., constant or linear). Such variable acceleration might have been more expected to result from higher-level factors (e.g., stimulus familiarity), which might arrive too late to interact with all processing stages, rather than the present manipulation.

The waxing and waning of acceleration that we observed during temporal integration is at odds with simplistic models of perceptual processing. In particular, models with few parameters, such as (drift diffusion) models of temporal preparation, which allow only for alterations of the rate at which sensory evidence accumulates increase and of the onset of this process (e.g., Vangkilde, Coull, & Bundesen, 2012; Seibold, Bausenhart, Rolke, & Ulrich, 2011; see also Jepma, Wagenmakers, & Nieuwenhuis, 2012), will be unable to account for the variable pattern we presently observed. Allowing some interaction between parameters would seem to be necessary.

More generally, this limitation also applies to traditional additive factors logic (Linden, 2007; Sternberg, 1969, 2001; Donders, 1868). In this framework, the chain of processing is divided into distinct, independent stages or modules, each of which is conceptualized as an independent computation, transforming input to output. Acceleration may act on each stage, reducing the time needed to complete that transformation, without affecting any other processing stage. The relationship between different stages is

also summative, so that subsequent computations in the perceptual and cognitive chain will commence sooner, until eventually the behavioral response is also quickened. Although attractive for its elegant simplicity, this framework cannot accommodate the variable effects that we found.

It may be noted here that our study is not the first to question the idea of independence between different processing stages. Under- and overadditive effects have previously emerged in dual-task situations, where the processing of multiple (conflicting) stimuli is required simultaneously (Ridderinkhof, van der Molen, & Bashore, 1995) and where multiple subtasks need to be chained (e.g., Sackur & Dehaene, 2009), but also in single-task foreperiod studies (e.g., Los & Schut, 2008). These findings also suggest that concurrent modulation of multiple stages can occur (Marti & Dehaene, 2017; see also Caplan, 2007, for an extended discussion). Recent stage-based models have incorporated this by allowing temporal variation within each stage and by using neurophysiological markers ("bumps") to define the stages as well as their number (van Maanen, Portoles, & Borst, 2021; Vidaurre, Cichy, & Woolrich, 2021; Vidaurre, Myers, Stokes, Nobre, & Woolrich, 2019; Anderson, Zhang, Borst, & Walsh, 2016). The loss of simplicity in these models may detract to some degree from the idea of a serial processing chain and make it harder to pinpoint modulatory factors therein. Overall, however, these more data-driven stage-based models may currently hold the most promise in explaining perceptual acceleration as well.

As a caveat, it must be noted that the stages we identified in the present data were not the result of systematic analyses of the EEG, because it was not our purpose to attempt such identification. We, therefore, do not want to overstate the stage-specific nature of the observed acceleration effects. In our study, the processing stages have an arbitrary element. Their main purpose was to provide a handle on different moments in what might as well be considered a continuous processing stream (cf. Figure 4C and D). Importantly, the conclusion that the representation of the missing element location exhibited varying degrees of acceleration across the interval under consideration is largely unaffected by whether stage boundaries might be drawn differently within.

Temporal Integration

The MET is traditionally used to measure visual temporal integration, and we indeed observed the associated pattern of results, in which increasing SOA resulted in fewer correct reports of the missing element location. The electrophysiological results provided an intriguing view on how temporal integration may be facilitated in the brain. To reiterate, the missing element location emerged sooner than would be expected on the basis of the SOA between the displays. This suggests that the processing of the first and second stimuli gets temporally "compressed" in the brain. This compression is not predicted by models of temporal integration, which generally assume that integration is mostly a consequence of temporal overlap or coincidence of the processing of the second display with lingering representations of the first display, referred to as visible persistence, rather than any perceptual acceleration (Loftus & Irwin, 1998; Dixon & Di Lollo, 1994; Hogben & di Lollo, 1974; Sperling, 1960). Nevertheless, the current results suggest that perceptual acceleration may cause increased temporal overlap between stimulus representations when processing rapid successive stimuli, which would increase the chance that they are temporally integrated. Furthermore, the early arrival of the (features of the) trailing stimulus may facilitate the perception of simultaneity and thereby enhance temporal integration as well. Whether this perceived simultaneity is an independent factor might be a topic for further study.

Conclusion

In the MET, we found that perception of the first display accelerates the processing of the second, which may contribute to the process of temporal integration. Temporal generalization analyses of the EEG patterns associated with the representation of the missing element showed that this acceleration is neither linear nor constant and varies from moment to moment in the perceptual processing chain. Although the results are still compatible with the general idea of a fixed chain of perceptual processing stages, they do suggest that attempts to isolate and time processing stage-specific effects may mischaracterize the actual flow of events.

Corresponding author: Elkan Akyürek, Department of Experimental Psychology, University of Groningen, Grote Kruisstraat 2/1, 9712 TS Groningen, The Netherlands, e-mail: e.g.akyurek@rug.nl.

Data Availability Statement

All data are openly available on osf.io/kftjw. The custom MATLAB code that reproduces all results in this manuscript is available on github.com/mijowolff/Accelerating-perception-during-temporal-integration. Supplemental Material can be accessed on this article's homepage: https://doi.org/10.1162/JOCN.a.2421.

Author Contributions

Michael J. Wolff: Conceptualization; Data curation; Formal analysis; Investigation; Methodology; Software; Validation; Writing—Original draft; Writing—Review & editing; Visualization. Elkan G. Akyürek: Conceptualization; Methodology; Project administration; Resources; Supervision; Writing—Original draft; Writing—Review & editing.

Diversity in Citation Practices

Retrospective analysis of the citations in every article published in this journal from 2010 to 2021 reveals a persistent pattern of gender imbalance: Although the proportions of authorship teams (categorized by estimated gender identification of first author/last author) publishing in the *Journal of Cognitive Neuroscience* (*JoCN*) during this period were M(an)/M = .407, W(oman)/M = .32, M/W = .115, and W/W = .159, the comparable proportions for the articles that these authorship teams cited were M/M = .549, W/M = .257, M/W = .109, and W/W = .085 (Postle and Fulvio, *JoCN*, 34:1, pp. 1–3). Consequently, *JoCN* encourages all authors to consider gender balance explicitly when selecting which articles to cite and gives them the opportunity to report their article's gender citation balance.

REFERENCES

Akyürek, E. G. (2025). Temporal integration as an adaptive process in visual perception, attention, and working memory. *Neuroscience & Biobehavioral Reviews*, *170*, 106041. https://doi.org/10.1016/j.neubiorev.2025.106041, PubMed: 39922439

Akyürek, E. G., Kappelmann, N., Volkert, M., & van Rijn, H. (2017). What you see is what you remember: Visual chunking by temporal integration enhances working memory. *Journal of Cognitive Neuroscience*, *29*, 2025–2036. https://doi.org/10.1162/jocn_a_01175, PubMed: 28777057

Akyürek, E. G., Schubö, A., & Hommel, B. (2010). Fast temporal event integration in the visual domain demonstrated by event-related potentials. *Psychophysiology*, *47*, 512–522. https://doi.org/10.1111/j.1469-8986.2010.00962.x, PubMed: 20136735

Anderson, J. R., Zhang, Q., Borst, J. P., & Walsh, M. M. (2016). The discovery of processing stages: Extension of Sternberg's method. *Psychological Review*, *123*, 481–509. https://doi.org/10.1037/rev0000030, PubMed: 27135600

Caplan, D. (2007). Experimental design and interpretation of functional neuroimaging studies of cognitive processes. *Human Brain Mapping*, *30*, 59–77. https://doi.org/10.1002/hbm.20489, PubMed: 17979122

Cichy, R. M., Pantazis, D., & Oliva, A. (2014). Resolving human object recognition in space and time. *Nature Neuroscience*, *17*, 455–462. https://doi.org/10.1038/nn.3635, PubMed: 24464044

Coull, J. T., & Nobre, A. C. (1998). Where and when to pay attention: The neural systems for directing attention to spatial locations and to time intervals as revealed by both PET and fMRI. *Journal of Neuroscience*, *18*, 7426–7435. https://doi.org/10.1523/JNEUROSCI.18-18-07426.1998, PubMed: 9736662

De Maesschalck, R., Jouan-Rimbaud, D., & Massart, D. L. (2000). The Mahalanobis distance. *Chemometrics and Intelligent Laboratory Systems*, *50*, 1–18. https://doi.org/10.1016/S0169-7439(99)00047-7

Di Lollo, V. (1977). Temporal characteristics of iconic memory. *Nature*, *267*, 241–243. https://doi.org/10.1038/267241a0, PubMed: 865614

Di Lollo, V. (1980). Temporal integration in visual memory. *Journal of Experimental Psychology: General*, *109*, 75–97. https://doi.org/10.1037/0096-3445.109.1.75, PubMed: 6445405

Dixon, P., & Di Lollo, V. (1994). Beyond visible persistence: An alternative account of temporal integration and segregation in visual processing. *Cognitive Psychology*, *26*, 33–63. https://doi.org/10.1006/cogp.1994.1002, PubMed: 8131379

Donders, F. C. (1868). Over de snelheid van psychische processen. *Onderzoekingen gedaan in het Physiologisch Laboratorium der Utrechtsche Hoogeschool*, *2*, 92–120.

Friston, K. (2005). A theory of cortical responses. *Philosophical Transactions of the Royal Society of London, Series B: Biological Sciences*, *360*, 815–836. https://doi.org/10.1098/rstb.2005.1622, PubMed: 15937014

Griffin, I. C., Miniussi, C., & Nobre, A. C. (2002). Multiple mechanisms of selective attention: Differential modulation of stimulus processing by attention to space or time. *Neuropsychologia*, *40*, 2325–2340. https://doi.org/10.1016/S0028-3932(02)00087-8, PubMed: 12417462

Harrison, W. J., Bays, P. M., & Rideaux, R. (2023). Neural tuning instantiates prior expectations in the human visual system. *Nature Communications*, *14*, 5320. https://doi.org/10.1038/s41467-023-41027-w, PubMed: 37658039

Hillyard, S. A., Teder-Sälejärvi, W. A., & Münte, T. F. (1998). Temporal dynamics of early perceptual processing. *Current Opinion in Neurobiology*, *8*, 202–210. https://doi.org/10.1016/S0959-4388(98)80141-4, PubMed: 9635203

Hogben, J. H., & di Lollo, V. (1974). Perceptual integration and perceptual segregation of brief visual stimuli. *Vision Research*, *14*, 1059–1069. https://doi.org/10.1016/0042-6989(74)90202-8, PubMed: 4428612

Jepma, M., Wagenmakers, E.-J., & Nieuwenhuis, S. (2012). Temporal expectation and information processing: A model-based analysis. *Cognition*, *122*, 426–441. https://doi.org/10.1016/j.cognition.2011.11.014, PubMed: 22197060

Jones, M. R., Moynihan, H., MacKenzie, N., & Puente, J. (2002). Temporal aspects of stimulus-driven attending in dynamic arrays. *Psychological Science*, *13*, 313–319. https://doi.org/10.1111/1467-9280.00458, PubMed: 12137133

Kandemir, G., & Olivers, C. (2024). Comparing neural correlates of memory encoding and maintenance for foveal and peripheral stimuli. *Journal of Cognitive Neuroscience*, *36*, 1807–1826. https://doi.org/10.1162/jocn_a_02203, PubMed: 38940724

King, J.-R., & Dehaene, S. (2014). Characterizing the dynamics of mental representations: The temporal generalization method. *Trends in Cognitive Sciences*, *18*, 203–210. https://doi.org/10.1016/j.tics.2014.01.002, PubMed: 24593982

Kirchner, H., & Thorpe, S. J. (2006). Ultra-rapid object detection with saccadic eye movements: Visual processing speed revisited. *Vision Research*, *46*, 1762–1776. https://doi.org/10.1016/j.visres.2005.10.002, PubMed: 16289663

Kleiner, M., Brainard, D., & Pelli, D. (2007). What's new in Psychtoolbox-3? *Perception*, *36*, 14.

Ledoit, O., & Wolf, M. (2004). Honey, I shrunk the sample covariance matrix. *Journal of Portfolio Management*, *30*, 110–119. https://doi.org/10.3905/jpm.2004.110

Linden, D. E. J. (2007). What, when, where in the brain? Exploring mental chronometry with brain imaging and electrophysiology. *Reviews in the Neurosciences*, *18*, 159–171. https://doi.org/10.1515/revneuro.2007.18.2.159, PubMed: 17593878

Lleras, A., Rensink, R. A., & Enns, J. T. (2005). Rapid resumption of interrupted visual search: New insights on the interaction between vision and memory. *Psychological Science*, *16*, 684–688. https://doi.org/10.1111/j.1467-9280.2005.01596.x, PubMed: 16137253

Loftus, G. R., & Irwin, D. E. (1998). On the relations among different measures of visible and informational persistence. *Cognitive Psychology*, *35*, 135–199. https://doi.org/10.1006/cogp.1998.0678, PubMed: 9570898

Los, S. A., & Schut, M. L. J. (2008). The effective time course of preparation. *Cognitive Psychology*, *57*, 20–55. https://doi.org/10.1016/j.cogpsych.2007.11.001, PubMed: 18255052

Luce, R. D. (1991). *Response times: Their role in inferring elementary mental organization*. Oxford University Press.

Mangun, G. R. (1995). Neural mechanisms of visual selective attention. *Psychophysiology*, *32*, 4–18. https://doi.org/10.1111/j.1469-8986.1995.tb03400.x, PubMed: 7878167

Mangun, G. R., & Hillyard, S. A. (1991). Modulations of sensory-evoked brain potentials indicate changes in perceptual processing during visual-spatial priming. *Journal of Experimental Psychology: Human Perception and Performance*, *17*, 1057–1074. https://doi.org/10.1037/0096-1523.17.4.1057, PubMed: 1837297

Markram, H., Lübke, J., Frotscher, M., & Sakmann, B. (1997). Regulation of synaptic efficacy by coincidence of postsynaptic APs and EPSPs. *Science*, *275*, 213–215. https://doi.org/10.1126/science.275.5297.213, PubMed: 8985014

Marti, S., & Dehaene, S. (2017). Discrete and continuous mechanisms of temporal selection in rapid visual streams. *Nature Communications*, *8*, 1955. https://doi.org/10.1038/s41467-017-02079-x, PubMed: 29208892

Marti, S., King, J.-R., & Dehaene, S. (2015). Time-resolved decoding of two processing chains during dual-task interference. *Neuron*, *88*, 1297–1307. https://doi.org/10.1016/j.neuron.2015.10.040, PubMed: 26627309

Mathewson, K. E., Fabiani, M., Gratton, G., Beck, D. M., & Lleras, A. (2010). Rescuing stimuli from invisibility: Inducing a momentary release from visual masking with pre-target entrainment. *Cognition*, *115*, 186–191. https://doi.org/10.1016/j.cognition.2009.11.010, PubMed: 20035933

Myers, N. E., Rohenkohl, G., Wyart, V., Woolrich, M. W., Nobre, A. C., & Stokes, M. G. (2015). Testing sensory evidence against mnemonic templates. *eLife*, *4*, e09000. https://doi.org/10.7554/eLife.09000, PubMed: 26653854

Oostenveld, R., Fries, P., Maris, E., & Schoffelen, J.-M. (2010). FieldTrip: Open source software for advanced analysis of MEG, EEG, and invasive electrophysiological data. *Computational Intelligence and Neuroscience*, *2011*, 156869. https://doi.org/10.1155/2011/156869, PubMed: 21253357

Palmer, S. E., Marre, O., Berry, M. J., & Bialek, W. (2015). Predictive information in a sensory population. *Proceedings of the National Academy of Sciences, U.S.A.*, *112*, 6908–6913. https://doi.org/10.1073/pnas.1506855112, PubMed: 26038544

Patel, S. H., & Azzam, P. N. (2005). Characterization of N200 and P300: Selected studies of the event-related potential. *International Journal of Medical Sciences*, *2*, 147–154. https://doi.org/10.7150/ijms.2.147, PubMed: 16239953

Polich, J. (2007). Updating P300: An integrative theory of P3a and P3b. *Clinical Neurophysiology*, *118*, 2128–2148. https://doi.org/10.1016/j.clinph.2007.04.019, PubMed: 17573239

Posner, M. I. (1980). Orienting of attention. *Quarterly Journal of Experimental Psychology*, *32*, 3–25. https://doi.org/10.1080/00335558008248231, PubMed: 7367577

Praamstra, P., Kourtis, D., Kwok, H. F., & Oostenveld, R. (2006). Neurophysiology of implicit timing in serial choice reaction-time performance. *Journal of Neuroscience*, *26*, 5448–5455. https://doi.org/10.1523/JNEUROSCI.0440-06.2006, PubMed: 16707797

Ridderinkhof, K. R., van der Molen, M. W., & Bashore, T. R. (1995). Limits on the application of additive factors logic: Violations of stage robustness suggest a dual-process architecture to explain flanker effects on target processing. *Acta Psychologica*, *90*, 29–48. https://doi.org/10.1016/0001-6918(95)00031-O

Rohenkohl, G., & Nobre, A. C. (2011). Alpha oscillations related to anticipatory attention follow temporal expectations. *Journal of Neuroscience*, *31*, 14076–14084. https://doi.org/10.1523/JNEUROSCI.3387-11.2011, PubMed: 21976492

Rouder, J. N., Speckman, P. L., Sun, D., Morey, R. D., & Iverson, G. (2009). Bayesian *t* tests for accepting and rejecting the null hypothesis. *Psychonomic Bulletin & Review*, *16*, 225–237. https://doi.org/10.3758/PBR.16.2.225, PubMed: 19293088

Sackur, J., & Dehaene, S. (2009). The cognitive architecture for chaining of two mental operations. *Cognition*, *111*, 187–211. https://doi.org/10.1016/j.cognition.2009.01.010, PubMed: 19306995

Seibold, V. C., Bausenhart, K. M., Rolke, B., & Ulrich, R. (2011). Does temporal preparation increase the rate of sensory information accumulation? *Acta Psychologica*, *137*, 56–64. https://doi.org/10.1016/j.actpsy.2011.02.006, PubMed: 21440239

Seibold, V. C., Fiedler, A., & Rolke, B. (2011). Temporal attention shortens perceptual latency: A temporal prior entry effect. *Psychophysiology*, *48*, 708–717. https://doi.org/10.1111/j.1469-8986.2010.01135.x, PubMed: 20883507

Seibold, V. C., & Rolke, B. (2014). Does temporal preparation speed up visual processing? Evidence from the N2pc. *Psychophysiology*, *51*, 529–538. https://doi.org/10.1111/psyp.12196, PubMed: 24611621

Spaak, E., Fonken, Y., Jensen, O., & de Lange, F. P. (2016). The neural mechanisms of prediction in visual search. *Cerebral Cortex*, *26*, 4327–4336. https://doi.org/10.1093/cercor/bhv210, PubMed: 26400919

Sperling, G. (1960). The information available in brief visual presentations. *Psychological Monographs: General and Applied*, *74*, 1–29. https://doi.org/10.1037/h0093759

Sternberg, S. (1969). The discovery of processing stages: Extensions of Donders' method. *Acta Psychologica*, *30*, 276–315. https://doi.org/10.1016/0001-6918(69)90055-9

Sternberg, S. (2001). Separate modifiability, mental modules, and the use of pure and composite measures to reveal them. *Acta Psychologica*, *106*, 147–246. https://doi.org/10.1016/S0001-6918(00)00045-7, PubMed: 11256336

Summerfield, C., & Egner, T. (2009). Expectation (and attention) in visual cognition. *Trends in Cognitive Sciences*, *13*, 403–409. https://doi.org/10.1016/j.tics.2009.06.003, PubMed: 19716752

Thorpe, S., Fize, D., & Marlot, C. (1996). Speed of processing in the human visual system. *Nature*, *381*, 520–522. https://doi.org/10.1038/381520a0, PubMed: 8632824

van Ede, F., Chekroud, S. R., Stokes, M. G., & Nobre, A. C. (2018). Decoding the influence of anticipatory states on visual perception in the presence of temporal distractors. *Nature Communications*, *9*, 1449. https://doi.org/10.1038/s41467-018-03960-z, PubMed: 29654312

van Ede, F., Chekroud, S. R., Stokes, M. G., & Nobre, A. C. (2019). Concurrent visual and motor selection during visual working memory guided action. *Nature Neuroscience*, *22*, 477–483. https://doi.org/10.1038/s41593-018-0335-6, PubMed: 30718904

van Maanen, L., Portoles, O., & Borst, J. P. (2021). The discovery and interpretation of evidence accumulation stages. *Computational Brain & Behavior*, *4*, 395–415. https://doi.org/10.1007/s42113-021-00105-2

Vangkilde, S., Coull, J. T., & Bundesen, C. (2012). Great expectations: Temporal expectation modulates perceptual processing speed. *Journal of Experimental Psychology: Human Perception and Performance*, *38*, 1183–1191. https://doi.org/10.1037/a0026343, PubMed: 22250866

VanRullen, R., & Thorpe, S. J. (2001). The time course of visual processing: From early perception to decision-making. *Journal of Cognitive Neuroscience*, *13*, 454–461. https://doi.org/10.1162/08989290152001880, PubMed: 11388919

Verleger, R., Jaśkowski, P., & Wascher, E. (2005). Evidence for an integrative role of P3b in linking reaction to perception.

Journal of Psychophysiology, *19*, 165–181. https://doi.org/10.1027/0269-8803.19.3.165

Vidaurre, D., Cichy, R. M., & Woolrich, M. W. (2021). Dissociable components of information encoding in human perception. *Cerebral Cortex*, *31*, 5664–5675. https://doi.org/10.1093/cercor/bhab189, PubMed: 34291294

Vidaurre, D., Myers, N. E., Stokes, M., Nobre, A. C., & Woolrich, M. W. (2019). Temporally unconstrained decoding reveals consistent but time-varying stages of stimulus processing. *Cerebral Cortex*, *29*, 863–874. https://doi.org/10.1093/cercor/bhy290, PubMed: 30535141

Vogel, E. K., & Machizawa, M. G. (2004). Neural activity predicts individual differences in visual working memory capacity. *Nature*, *428*, 748–751. https://doi.org/10.1038/nature02447, PubMed: 15085132

Woldorff, M. G., Fox, P. T., Matzke, M., Lancaster, J. L., Veeraswamy, S., Zamarripa, F., et al. (1997). Retinotopic organization of early visual spatial attention effects as revealed by PET and ERPs. *Human Brain Mapping*, *5*, 280–286. https://doi.org/10.1002/(SICI)1097-0193(1997)5:4<280::AID-HBM13>3.0.CO;2-I, PubMed: 20408229

Wolff, M. J., Ding, J., Myers, N. E., & Stokes, M. G. (2015). Revealing hidden states in visual working memory using electroencephalography. *Frontiers in Systems Neuroscience*, *9*, 123. https://doi.org/10.3389/fnsys.2015.00123, PubMed: 26388748

Wolff, M. J., Jochim, J., Akyürek, E. G., Buschman, T. J., & Stokes, M. G. (2020). Drifting codes within a stable coding scheme for working memory. *PLoS Biology*, *18*, e3000625. https://doi.org/10.1371/journal.pbio.3000625, PubMed: 32119658

Wolff, M. J., Jochim, J., Akyürek, E. G., & Stokes, M. G. (2017). Dynamic hidden states underlying working-memory-guided behavior. *Nature Neuroscience*, *20*, 864–871. https://doi.org/10.1038/nn.4546, PubMed: 28414333

Zucker, R. S., & Regehr, W. G. (2002). Short-term synaptic plasticity. *Annual Review of Physiology*, *64*, 355–405. https://doi.org/10.1146/annurev.physiol.64.092501.114547, PubMed: 11826273